Magnetic linear dichroism in Gd 4f and 4d photoemission of magnetic interfaces

1999 J. Phys.: Condens. Matter 11 3431

(http://iopscience.iop.org/0953-8984/11/17/302)

J. Phys.: Condens. Matter **11** (1999) 3431–3442. Printed in the UK PII: S0953-8984(99)01143-1

Magnetic linear dichroism in Gd 4f and 4d photoemission of magnetic interfaces

Giancarlo Panaccione†, Piero Torelli‡, Giorgio Rossi‡, Gerrit van der Laan§, P Prieto‖¶ and F Sirotti‖

† INFM, Istituto Nazionale per la Fisica della Materia, APE Project, c/o Sincrotrone Trieste, I-34012 Basovizza (Trieste), Italy
‡ INFM, Istituto Nazionale per la Fisica della Materia, Unità di Modena, Dipartimento di Fisica dell'Università di Modena e Reggio Emilia, I-41000 Modena, Italy
§ Daresbury Laboratory, Warrington WA4 4AD, UK
‖ Laboratoire pour l'Utilisation du Rayonnement Electromagnétique LURE, CNRS-CEA-MESR, F-91405 Orsay, France

Received 21 January 1999, in final form 17 March 1999

Abstract. We present a combined experimental and theoretical study of magnetic linear dichroism in the angular distribution (MLDAD) of Gd 4f and 4d core level photoemission. Expressions are given for the spectral shape and photon energy dependence by using the method of fundamental spectra. The results are compared with experimental data for a thin Gd layer on Fe(100) and for a Fe/Gd/Fe interface. Compared to magnetic circular dichroism (MCD) in 4f photoemission, the MLDAD is much smaller and undergoes a sign change around 80 eV kinetic energy. We show that for 4f and 4d emission the spectral shapes of the MLDAD and MCD are in principle different, but in practice these differences are too small to observe.

1. Introduction

In recent years, photoemission using polarized x-rays has become an important method to study magnetic surfaces and thin films. The prime step in the analysis of the photoelectron distribution in a specific experimental geometry, as determined by the photon energy, kinetic energy and the emission angle, is the separation of the transition probability into a physical and a geometric part [1]. In an atomic model, neglecting solid state and diffraction effects, we can consider three principal vectors: namely, the magnetization direction, $\boldsymbol{M}$; the light polarization, $\boldsymbol{P}$; and the electron emission direction, ε. When these vectors are neither coplanar nor mutually perpendicular, the geometry will have a chirality, i.e. a certain handedness. This means that if one of the vectors is reversed, such as the magnetization or the light helicity, the opposite handedness is obtained, accompanied by a change in the photoemission signal, i.e. dichroism is observed. By using the chirality in the photoemission experiment, it becomes possible to measure with linear polarization the magnetic dichroism which is otherwise only accessible by circularly polarized light. This technique is called magnetic linear dichroism in the angular distribution (MLDAD) [2] and provides a versatile method to study magnetic surfaces, thin films and overlayers of transition metal (TM) and rare earth (RE) systems. RE have been studied mainly by means of magnetic circular dichroism (MCD) and spin polarized

¶ Present address: Departemento de Fisica Aplicada, Facultad de Ciencias, Universitad Autonoma de Madrid, 28049 Cantoblanco, Madrid, Spain.

0953-8984/99/173431+12$19.50

photoemission techniques [3–6]. Spin detection of the photoelectrons, although interesting in its own right, falls beyond the scope of the current paper. The MLDAD technique is a straightforward photoemission experiment requiring only linearly polarized x-rays and has an easy-to-analyse angular dependence: these characteristics are strongly advantageous, both experimentally and theoretically. Recent experiments have demonstrated that

(i) in agreement with theoretical predictions, sizeable MLDAD effects from the Gd 4f core level are attainable in the photon energy region below 50 eV [7];
(ii) the MLDAD up-down feature is determined by the orbital magnetic moment of the core hole, revealing the coupling between different elements in a composite interface [7];
(iii) MLDAD experiments were able to explore of the nature of resonant photoemission processes using the giant 4d $\rightarrow$ 4f resonance [8].

This is possible because the chirality of the MLDAD originates from a vectorial geometry and is not intrinsic, such as in MCD where the circular polarization of the x-rays imposes a handedness on the experiment.

In this paper we report on a detailed comparison between experiment and theory for Gd MLDAD on various systems, such as the Gd 4f core level in the Gd/Fe(100) interface and the 4d core levels of the Gd/Fe and Fe/Gd/Fe interface. The motivation for this analysis is twofold. Firstly, from spectroscopic viewpoint and in terms of fundamental spectra, information can be obtained about the parameters that play a major role in the magnetic signal. Secondly, the TM/RE interface, being representative of itinerant versus localized magnetic behaviour, presents several interesting aspects of the coupling between two different magnetic materials.

2. Experimental details

Measurements were performed on the Swiss–French beamline SU3 and on beamline SU7 at the SuperAco storage ring in LURE (Orsay). In both cases, the electron energy analysers were at 45° with respect to the direction of the linearly polarized synchrotron radiation impinging onto the sample from standard planar undulators. The angular acceptance was $\pm 1^\circ$ (SU3) and $\pm 22^\circ$ (SU7). The overall energy resolution was $\sim$ 100 meV (SU3) and $\sim$ 300 meV (SU7). The substrate was an oriented Fe3%S (100) single crystal in the case of the Gd/Fe(100) and a soft magnetic ribbon (Vitrovac) for the Gd/Fe and Fe/Gd/Fe interfaces, both mounted to close the gap of a soft iron yoke [9, 10]. Clean substrate surfaces were prepared by Ar^+ ion sputtering. Gd was evaporated from a tungsten basket with a typical deposition rate of 0.2 Å min^{-1} with a pressure below 2×10^{-10} mbar. The base pressure was 8×10^{-11} mbar. The thickness of the deposited layers was monitored by a quartz crystal oscillator and verified by the ratio between the Gd 4f and Fe 3p photoemission intensities. Valence band photoemission spectra were used to monitor the surface cleanliness during the measurements, controlling the 2p-derived oxygen states at $\sim$ 6 eV below the Fermi level. The substrate was magnetically saturated by current pulses through the windings of an electromagnet and all spectra were measured in remanence, under normal emission (Vitrovac substrate) and in normal incidence (Fe(100) substrate). Photoelectron diffraction effects can strongly influence both the lineshape and the magnitude of the MLDAD as shown in recent experiments [11, 12]. For this reason, the Fe(100) surface was deliberately not annealed, in order to reduce any structure related effects. The MLDAD magnetic asymmetry is defined (see [10]) as $J_{\mathrm{ASYM}} = (J_{\mathrm{up}} - J_{\mathrm{down}})/(J_{\mathrm{up}} + J_{\mathrm{down}}) = J_{\mathrm{MLDAD}}/J_{\mathrm{SUM}}$, where $J_{\mathrm{up(down)}}$ is the photoemission intensity measured for the imposed magnetization in the up (down) direction with respect to the scattering plane, defined by the light polarization, $\boldsymbol{P}$, and the electron emission direction, ε. This experimental geometry defines the chirality and, by reversing the

magnetization with respect to the scattering plane, a MLDAD dichroism is obtained, as shown, for example, in figure 1, which gives the case of a 2 Å Gd film on Fe(100) taken at $h\nu = 70$ eV. At this photon energy the Gd 4f core level displays an intense MLDAD, whereas the valence band reveals a very weak dichroism.

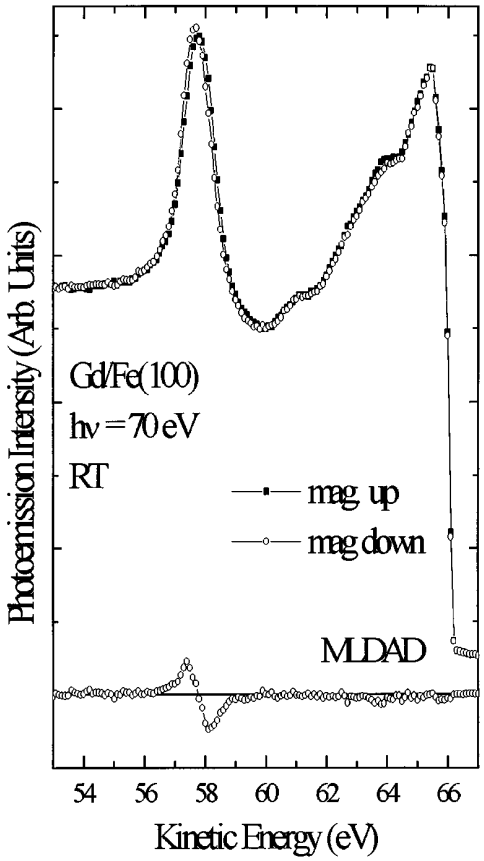

Figure 1. Top: magnetization dependent spectra (○ and ■) and bottom: MLDAD (○) of Gd 4f core level and valence band photoemission for 2 Å of Gd on Fe(100) at $h\nu = 70$ eV. The weak shoulder at around 61 eV kinetic energy is due to an O 2p contribution.

3. Theory

Although for the p shell an analytical expression for the angular dependent photoemission can be obtained by explicit evaluation of the transition probability [13], such an approach becomes rather complicated for an f shell. Therefore, we will employ here the powerful method of the fundamental spectra and multipole moments as described previously in a series of three papers [14–16].

In cylindrical symmetry, the dipole transition probability for angular dependent spin integrated photoemission J^a, in the direction ε for light specified by moment a and

polarization $\boldsymbol{P}$ from an atom with multipole moment along $\boldsymbol{M}$, can be written as [16]

$$4\pi J^a(\boldsymbol{M}, \boldsymbol{P}, \varepsilon) = \sum_{x,b} I^x Z^{cc'}_{xab}(\boldsymbol{M}, \boldsymbol{P}, \varepsilon) \tag{1}$$

where the angle and energy dependent term is given as

$$Z^{cc'}_{xab}(\boldsymbol{M}, \boldsymbol{P}, \varepsilon) = U^{xab}(\boldsymbol{M}, \boldsymbol{P}, \varepsilon) \sum_{cc'} A^{cc'}_{xab} R_c R_{c'} \mathrm{e}^{\mathrm{i}\delta} \tag{2}$$

where R_c is the energy dependent radial dipole matrix element and $\delta = \delta_c - \delta_{c'}$ is the phase difference for excitation to the two continuum states with orbital momentum $c = l \pm 1$, with interference between the two final state channels c and c'. The I^x are the fundamental spectra which give the probability for removal of an electron with moment x [14]. These spectra are independent of the photon energy and geometry and are determined by the physical properties of the atoms. The isotropic I^0 spectrum is independent of the external field. A spectrum with an odd value of x involves an oriented orbital moment and, with an even value of x, involves a charge distribution. Each I^x produces a limited set of angular distributions U^{xab} with contributions from each channel as the 9-j symbol $A^{cc'}_{xab}$ times the radial matrix elements and phase shifts, where x, a and b are the moments of the atomic shell, the light and the photoelectron distribution, respectively. In this notation $a = 0$ means isotropic light, i.e. the sum of intensities obtained with right-circularly ($q = -\Delta m = -1$), Z-linearly ($q = -\Delta m = 0$**)** and left-circularly ($q = -\Delta m = +1$) polarized radiation. Isotropic light is independent of the polarization $\boldsymbol{P}$. By $a = 1$ we denote circular dichroism, which is the difference in intensities for left and right circularly polarized light with the helicity vector along $\boldsymbol{P}$. By $a = 2$ we denote linear dichroism: the intensities for light polarized in two perpendicular directions perpendicular to $\boldsymbol{P}$ ($q = 1$ and -1) minus twice the intensity for light polarized along $\boldsymbol{P}$($q = 0$). The moment b of the photoemission distribution must be even due to parity; $b = 0$ represents an isotropic emission, $b = 2$ represents a quadrupolar emission distribution, etc. Conservation of the angular momentum requires a triangular condition $b = |a - x|, \cdots, a + x$. When $x + a$ is even, the 9-j symbol $A^{cc'}_{xab}$ is symmetric in c and c' so that

$$R_c R_{c'} \left(\mathrm{e}^{\mathrm{i}\delta} + \mathrm{e}^{-\mathrm{i}\delta}\right) = 2 R_c R_{c'} \cos\delta. \tag{3}$$

When $x + a$ is odd A is imaginary and antisymmetric in c and c' and

$$R_c R_{c'} \left(\mathrm{e}^{\mathrm{i}\delta} - \mathrm{e}^{-\mathrm{i}\delta}\right) = 2\mathrm{i} R_c R_{c'} \sin\delta. \tag{4}$$

The waves, with $x + a$ being odd, can only be measured in a chiral geometry, i.e. where $\boldsymbol{M}$, $\boldsymbol{P}$ and ε are neither coplanar nor mutually perpendicular. Using the aforementioned triangle relations, we obtain for the isotropic, circular dichroism and linear dichroism

$$4\pi J^0 = \sum_{x\in \text{ even } \{0\cdots 2l\};b=x} I^x Z_{x0b} \tag{5}$$

$$4\pi J^1 = \sum_{x\in\{1\cdots 2l\};b\in \text{ even } \{x-1\cdots x+1\}} I^x Z_{x1b} \tag{6}$$

$$4\pi J^2 = \sum_{x\in\{0\cdots 2l\};b\in \text{ even } \{x-2\cdots x+2\}} I^x Z_{x2b} \tag{7}$$

respectively, which shows that we are usually dealing with a sum over several terms.

In the following, we will only derive expressions for f shell emission; those for d shell emission can be obtained in a similar way. Adopting the MLDAD geometry, with

$\angle(\boldsymbol{M},\boldsymbol{P}) = \pi/2$, $\angle(\boldsymbol{M},\varepsilon) = \pi/2$ and $\phi = \angle(\boldsymbol{P},\varepsilon) = \{0, \pi/2\}$, and using the tables in [16], the explicit expression for the photoemission intensity from the f shell is obtained as

$$\begin{aligned}4\pi J(\phi,\pm M) = {}& \tfrac{1}{98} I^0 \left[15R_d^2 + 12R_dR_g\cos\delta + 22R_g^2 + \left(3R_d^2 + 36R_dR_g\cos\delta + 10R_g^2\right)\cos 2\phi\right] \\ & + \tfrac{5}{1176} I^2 \left[45R_d^2 - 6R_dR_g\cos\delta + 59R_g^2 + \left(-9R_d^2 + 102R_dR_g\cos\delta + 10R_g^2\right)\cos 2\phi\right] \\ & + \tfrac{9}{8624} I^4 \left[50R_d^2 + 26R_dR_g\cos\delta + 71R_g^2 + \left(4R_d^2 + 118R_dR_g\cos\delta + 25R_g^2\right)\cos 2\phi\right] \\ & + \tfrac{5}{51744} I^6 \left[54R_d^2 + 102R_dR_g\cos\delta + 89R_g^2 + \left(36R_d^2 + 138R_dR_g\cos\delta + 71R_g^2\right)\cos 2\phi\right] \\ & \pm \tfrac{1}{112}\left(72I^1 + 28I^3 + 5I^5\right) R_dR_g\sin\delta\sin 2\phi \end{aligned} \tag{8}$$

where R_d and R_g are the radial-matrix elements for photoemission from the 4f shell to the εd and εg continuum states. The difference spectrum is

$$4\pi J^{\text{f shell}}_{\text{MLDAD}} = 4\pi J(\phi, M) - 4\pi J(\phi, -M) = \tfrac{1}{56}\left(72I^1 + 28I^3 + 5I^5\right) R_dR_g\sin\delta\sin 2\phi. \tag{9}$$

For comparison, the explicit expression for the photoemission intensity from the p shell is

$$\begin{aligned}4\pi J(\phi,\pm M) = {}& \tfrac{1}{36}\left(2I^0 + I^2\right)\left[2R_s^2 + 2R_sR_d\cos\delta + 5R_d^2 + \left(6R_sR_d\cos\delta + 3R_d^2\right)\cos 2\phi\right] \\ & \pm \tfrac{1}{2} I^1 R_sR_d\sin\delta\sin 2\phi \end{aligned} \tag{10}$$

resulting in a difference spectrum

$$4\pi J^{\text{p shell}}_{\text{MLDAD}} = I^1 R_sR_d\sin\delta\sin 2\phi. \tag{11}$$

Inspection shows that for both shells the azimuthal dependence of the photoemission is similar. For the sum and difference spectrum we have

$$J_{\text{SUM}} = a_1 + a_2\cos 2\phi \tag{12}$$

$$J_{\text{MLDAD}} = a_3\sin 2\phi. \tag{13}$$

The coefficients a_1 and a_2 depend only on I^x with $x \in (\text{even} \leqslant 2l)$, R_c^2, $R_{c'}^2$ and $R_cR_{c'}\cos\delta$, while the coefficient $a_3$depends only on I^x with $x \in (\text{odd} \leqslant 2l)$ and $R_cR_{c'}\sin\delta$. Thus the MLDAD spectrum contains only magnetic contributions and the angle-integrated signal vanishes. The sum spectrum depends only on the charge distribution, while magnetic contributions cancel.

The fundamental spectra for Gd 4f are given in figure 3 of [16] and those for Fe 3p are given in figure 9 in [17]. Figure 2 shows the experimental (taken at 40 eV photon energy) and the calculated MLDAD spectrum (upper panel) compared to the separate contributions of the I^1, I^3 and I^5 spectra. The high BE lobe is a bit sharper in the MLDAD, but the differences are small. The change in the MLDAD line shape due to the I^3 and I^5 contributions is relatively small ($\sim 10\%$) and difficult to resolve under the present experimental conditions. The theoretical and experimental MLDAD spectra agrees very well in terms of lineshape.

It is noted that the photoemission spectrum measured in MCD, i.e. in a non-chiral geometry, also depends on the spectra I^x with odd x, but as a different linear combination and with a different angular dependence. Therefore, the shape of the MLDAD spectrum is the same as the MCD spectrum when only the I^1 spectrum is present, i.e. in the case of p emission. However, for the d and f shell the contributions of the higher I^x spectra are often small so that the MLDAD will still resemble the MCD spectrum. Taking for simplicity only the angle integrated MCD signal, i.e. $b = 0$, we obtain for the f shell

$$\frac{J_{\text{MCD}}}{J_{\text{SUM}}} = \frac{9\left(3R_d^2 - 4R_g^2\right) I^1}{6\left(3R_d^2 + 4R_g^2\right) I^0 + \left(9R_d^2 + 5R_g^2\right) I^2}. \tag{14}$$

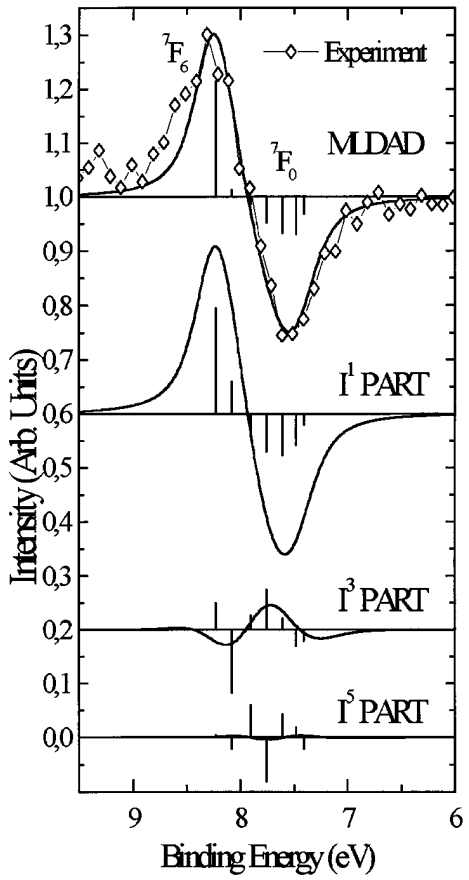

Figure 2. Top: theoretical (full curve) and experimental (◇, $h\nu = 40$ eV) Gd 4f MLDAD spectrum, compared to the contributions of the I^1, I^3 and I^5 spectra. Convolution as in [15]. The vertical bars show the heights and positions of the ^7F multiplet states.

In reality, we will always detect the electrons within a distinct angular acceptance cone, so that $b \neq 0$ terms also have to be included, which will lead to a strong angular dependence. In angle integrated MCD the interference terms disappear and contributions from R_g and R_d have an opposite sign. Since R_g is always much larger than R_d, the energy dependence of the MCD asymmetry is less than for the MLDAD.

4. Calculations

The kinetic energy dependence of the radial-matrix elements and phase factor were obtained using Cowan's code [18]. Their values for the $^7F_6$ level of the Gd $4f^6$ final state at an azimuthal angle of $\pi/4$ are displayed in figure 3. With the help of equation (9), we obtain the energy dependence of the MLDAD, which is given in figure 4, and division by the sum spectrum gives the asymmetry. The signal of the sum spectrum decreases strongly above 100 eV which makes the asymmetry relatively stronger. However, for accurate measurements, the signal becomes quite weak at these energies. At low energies the matrix element for the εg channel is three times larger than that of the εd channel, which increases to eight times at

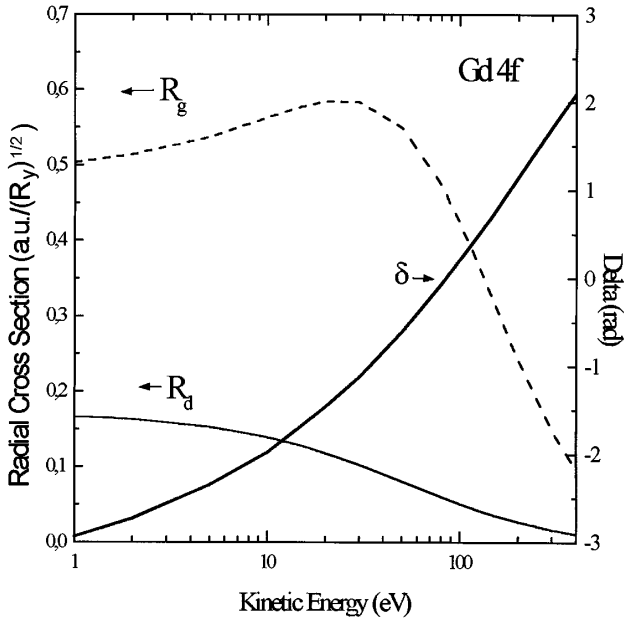

Figure 3. Kinetic energy dependence of the radial matrix elements R_d (full curve) and R_g (dashed curve) for photoemission from the Gd 4f to the εd and εg continuum states and the phase difference δ (full curve).

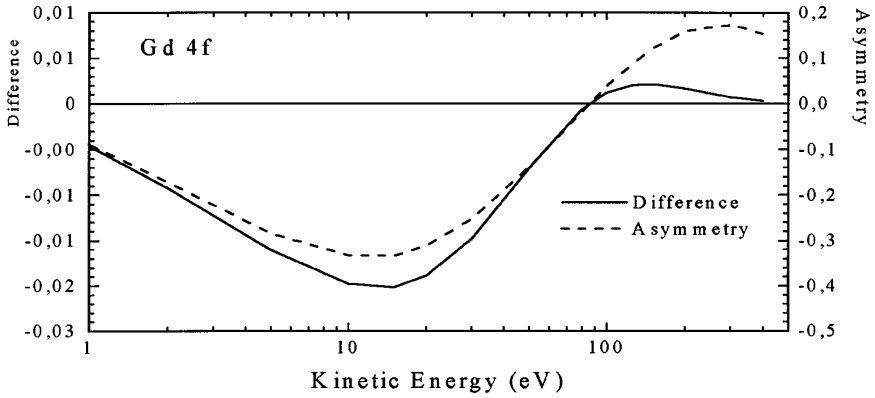

Figure 4. Kinetic energy dependence of the MLDAD difference (full curve) and asymmetry (dashed curve) signal for Gd 4f photoemission.

energies around 100 eV. This already tells us that the MLDAD asymmetry can never reach very high values, but it can still be above above 0.2. The MLDAD will be at maximum when $\delta \rightarrow (n+1/2)\pi$, which occurs near 20 eV and near 300 eV kinetic energy. A maximum value of 0.34 for the 4f asymmetry is obtained around 10–20 eV kinetic energy. The MLDAD vanishes when $\delta \rightarrow n\pi$, which occurs around 80 eV kinetic energy where $\delta = 0$. In the calculation we have not included the resonant photoemission from the 4d$\rightarrow$ 4f absorption around 140–150 eV, which has a strong effect on the cross-section, phase factor and angular dependence.

The 4d absorption can remove the chirality in the experimental geometry, thereby reducing the MLDAD asymmetry [8]. For the Gd 4d photoemission the spectra were calculated in the same way and with the same parameters as in [19].

Results for the Fe 3p photoemission have been given in figure 1 of [13], where the same sign convention was used. The maximum asymmetry occurs around 70 eV kinetic energy and is much larger than in the case of the Gd 4f photoemission, because the two emission channel have comparable radial-matrix elements.

The comparison between theory, as given in figure 4, and experimental results is presented in figure 5. An overall agreement with the calculation is found, confirming the reversal of the Gd 4f MLDAD sign at 120 eV kinetic energy. The Gd 4f photoemission spectra measured at $h\nu = 100$ eV and 200 eV, in the insets of figure 5, clearly illustrate the reversal of the MLDAD signal. The peak to peak J_{MLDAD} measured at $h\nu = 40$ eV, corresponding to figure 2, gives, after background subtraction, a J_{MLDAD} of $\sim$ 40% [7]. However, the experimental MLDAD asymmetry appears to be smaller than the theoretical prediction, which might be due to an incomplete saturation of the Gd film, since the measurements were performed at room temperature. At all measured photon energies we found that

(i) the magnetization averaged photemission spectra did not show any changes in the line shape;
(ii) the Gd 4f MLDAD spectrum always resembled the theoretical spectrum given in figure 2(a).

This suggests that photoelectron diffraction effects in the line shape are negligible under the given experimental conditions.

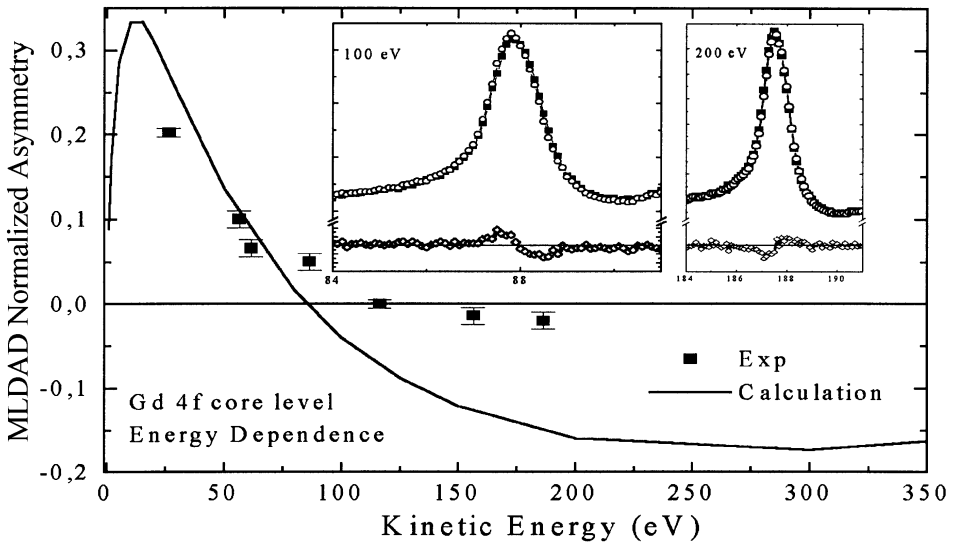

Figure 5. Theoretical (full curve) and experimental (■ with error bars) kinetic energy dependence of the MLDAD asymmetry for Gd 4f photoemission. The experimental values correspond to the energy dependence of the negative lobe of the MLDAD in figure 1. The value of the error bar also includes the reduction of the magnetic signal due to contamination. The insets show the magnetization dependent spectra of the Gd 4f and the corresponding MLDAD at $h\nu$ = 100 eV and 200 eV, showing the reversal of the MLDAD sign.

5. Magnetic coupling of Fe and Gd

5.1. Gd/Fe(100)

Figure 6(a) shows the Gd 4f magnetization dependent spectra and corresponding MLDAD taken at $h\nu$ = 40 eV. Figure 6(b) shows the Fe 3p MLDAD spectra, normalized to the same height, for the clean Fe(100) substrate and the Fe(100) top layers underneath the Gd film. The MLDAD signs are opposite for Gd and Fe. The Fe 3p MLDAD corresponding to the Fe at the interface Gd/Fe is shifted by $\sim 200 \pm 20$ meV towards higher kinetic energy. This chemical shift reflects the large electronegativity difference in the Gd–Fe bonding. Furthermore, the magnetic signal from the top layer of Gd is quickly lost as the thickness exceeds a few ångströms, confirming previous findings about the decrease of the Curie temperature value. A detailed analysis of the changes in magnetic properties at the Gd/Fe interface can be found elsewhere [20].

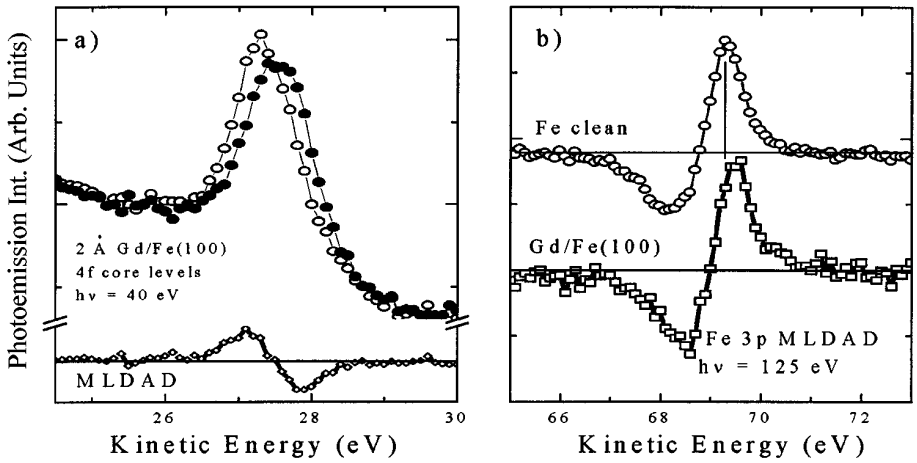

Figure 6. (a) Top: magnetization dependent spectra (○ and ●) and bottom: MLDAD (◊) of the Gd 4f photoemission for 2 Å of Gd on Fe(100) at $h\nu$ = 40 eV. (b) Comparison between the Fe 3p MLDAD of the clean Fe(100) surface (○) and the Fe 3p MLDAD (□) at $h\nu$ = 125 eV for the same Gd/Fe(100) interface as for (a). The vertical line, marking the energy position of the maximum, shows a shift of $\sim 200 \pm 20$ meV.

From spin resolved Auger spectroscopy [5] and spin resolved photoemission [6] it is known that the magnetic moments of Fe and Gd are coupled antiferromagnetic, so that the MLDAD signatures should be opposite for the Fe 3p and Gd 4f levels, taking into account the energy dependence, the radial-matrix elements, the phase factors and the sign of the I^x spectra. As shown in [14], the I^1 signal is proportional to the expectation value of the core hole orbital moment. The $^7F_6$ level (cf figure 2) corresponds to a positive orbital moment and the $^7F_0$ corresponds to a negative orbital moment. Moreover, because the spin and orbit prefer to be coupled antiparallel for the less than half filled $4f^6$, it is positive for the $^7F_6$ level and negative for the $^7F_0$ level, if we define the sign of the orbital moment positive when it is parallel to the ground-state spin. In the case of the Fe 3p final state, with only a single hole in the 3p shell, the spin and the orbit prefer to be coupled parallel. From this, we can conclude that when the MLDAD signatures are the same for the Fe 3p and Gd 4f levels, their *total* magnetic moments

are coupled ferromagnetic. Experimental results show therefore that

(i) the Gd film is coupled antiparallel to the Fe substrate and
(ii) the MLDAD up-down feature is governed by the orbital moment [7].

5.2. Gd/Fe and Fe/Gd/Fe

MLDAD experiments performed by subsequent evaporation of Gd and Fe on a soft magnetic driver reveal the thickness and temperature dependence of the Gd/Fe interface. As for the Gd/Fe(100), magnetization dependent spectra show an absence of MLDAD at 300 K for a 4 ML Gd film on Fe. This is the case for the MLDAD of the Gd 4d core level in figure 7. However, a sizeable MLDAD effect is found as soon as the temperature decreases (left panel of figure 7). For thicker layers, measured at the same temperature, the MLDAD goes rapidly to zero. On the other hand, a deposition of Fe, to produce a Fe/Gd/Fe trilayer system firmly coupled by the exchange interaction of the two Fe layers, shows an intense magnetic signal even at room temperature, i.e. in the range of temperature in which a thick Gd film without cap shows no MLDAD. The result is shown in figure 8 for the Gd 4d magnetization dependent spectra in a trilayer 3 ML Fe/2 ML Gd/20 ML Fe, taken at $h\nu$ = 320 eV. The comparison between experimental MLDAD and calculation [19] is presented in figure 9. The detailed structure of the theoretical MLDAD signal is not completely resolved in the experiment due to the limiting experimental resolution. Nevertheless, an overall agreement is found in the spectral structure with shoulders visible in the multiplet at low binding energy.

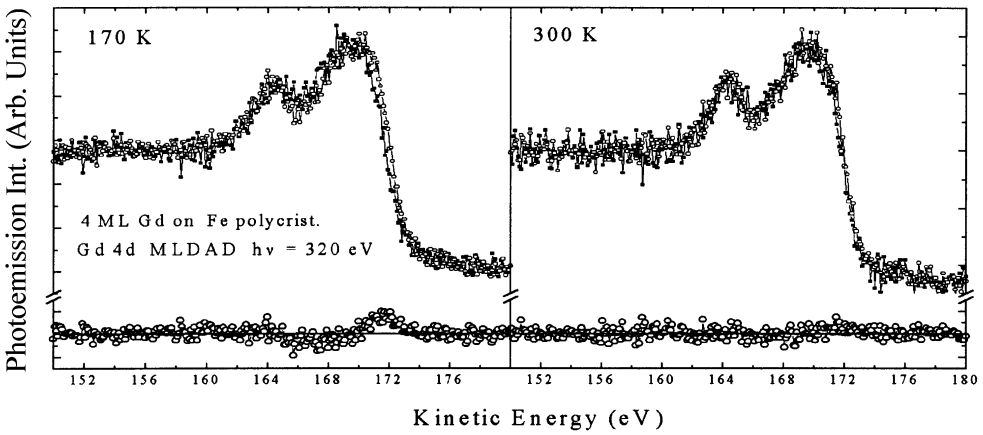

Figure 7. Top: magnetization dependent spectra (○ and ■) and bottom: MLDAD (○) of Gd 4d core level photoemission for 4 ML of Gd on polycristalline Fe at $h\nu$ = 320 eV for 170 K (left panel) and 300 K (right panel). There is no MLDAD signal at 300 K, but a clear magnetic signal arises at low temperature.

6. Conclusions

We have demonstrated that there is good agreement between experiment and theory for the MLDAD of the Gd 4f and 4d as well as for Fe 3p core level photoemission. Also the kinetic energy dependence of the Gd 4f asymmetry is in good agreement with the theory. From the comparison of the MLDAD signatures for the Gd 4f and Fe 3p we find an antiferromagnetic coupling between the two materials, which implies that the MLDAD up-down feature is

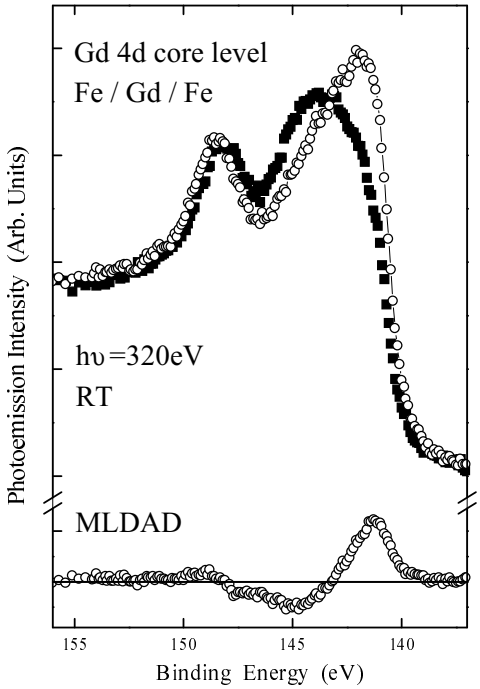

Figure 8. Top: magnetization dependent spectra (○ and ■) and bottom: MLDAD (○) of Gd 4d core level photoemission for a trilayer 3 ML Fe/2 ML Gd/20 ML Fe, grown on Vitrovac soft magnetic driver 4 ML of Gd on polycristalline Fe ($h\nu$ = 320 eV).

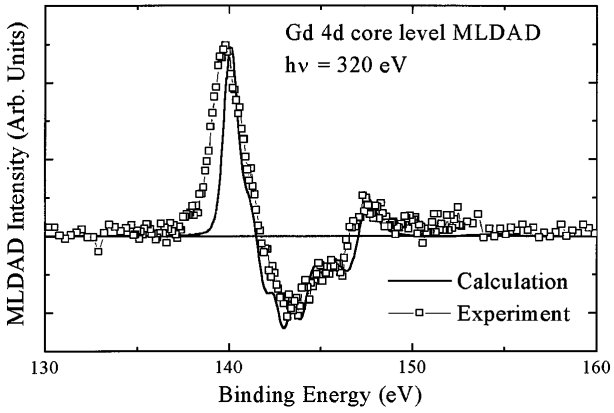

Figure 9. Comparison between the theoretical (full curve) and experimental (□, as in figure 8) Gd 4d MLDAD curve ($h\nu$ = 320 eV).

determined by the orbital magnetic moment. This means that the MLDAD measures the orbital moment of the created core-hole state. The comparison between experimental and the calculations has been instrumental in deriving this result, for which one has to take into account all parameters that play a role in the MLDAD signal and energy dependence. In a situation where the core-hole state is firmly coupled to the valence band spin by exchange interaction and spin-orbit coupling, such as in Fe, it will also be a good measure for the spin moment,

via the analysis of the width of the splitting, with the assumption that spin-orbit coupling is constant and a linear variation of the mean spin field. Also, for the Gd 4d, the MLDAD shows a strong resemblance with previously obtained MCD spectra, which indicates that the contribution of the I^3 spectra is small, just as in the case of the 4f emission. An improved level of experimental accuracy would be required to detect and exploit the difference between MCD and MLDAD. This is expected to be available in the near future from third generation synchrotron radiation facilities. If the I^3 contribution could be separated from the dominant I^1 contribution, it would give information on the magnetic moment contribution due to spin-orbit coupling of the spin with the charge multipole moment.

These features of the MLDAD open up new possibilities of quantitative magnetic measurements, by combining information about

(i) the long-range magnetic order at the surface (via the value of the asymmetry);
(ii) the chemical selectivity of the photoemission technique;
(iii) the analysis of the coupling between different elements;
(iv) a measurement of the magnetic moment (via the splitting value in TM).

Acknowledgment

Thanks are due to M Sacchi for fruitful discussions.

References

[1] For a simple review, see e.g. van der Laan G 1995 Dichroic photoemission for pedestrians *Core Level Spectroscopies for Magnetic Phenomena: Theory and Experiment* ed P Bagus *et al* (New York: Plenum) p 153
[2] Roth Ch, Hillebrecht F U, Rose H and Kisker E 1993 *Phys. Rev. Lett.* **70** 3479
Roth Ch, Rose H, Hillebrecht F U and Kisker E 1993 *Solid State Commun.* **86** 647
[3] For a review article, see e.g. Starke K, Navas E, Arenholz E and Kaindl G 1996 *Spin-Orbit-Influenced Spectroscopies of Magnetic Solids (Lecture Notes in Physics vol 466)* ed H Ebert and G Schütz (Berlin: Springer) and references therein
[4] Arenholz E, Navas E, Starke K, Baumgarten L and Kaindl G 1995 *Phys. Rev.* B **51** 8211
[5] Taborelli M, Allenspach R, Boffa G and Landolt M 1986 *Phys. Rev. Lett.* **56** 2869
Taborelli M, Allenspach R and Landolt M 1986 *Phys. Rev.* B **34** 6112
[6] Carbone C and Kisker E 1987 *Phys. Rev.* **B36** 1280
Carbone C, Rochow R, Braicovich L, Jungblut R, Kachel T, Tillmann D and Kisker E 1990 *Phys. Rev.* B **41** 3866
[7] Panaccione G, Torelli P, Rossi G, van der Laan G, Sacchi M and Sirotti F 1998 *Phys. Rev.* B **58** R5916
[8] Mishra S R, Cummins T R, Waddil G D, Gammon W J, van der Laan G, Goodman K W and Tobin J G 1998 *Phys. Rev. Lett.* **81** 1306
[9] Sirotti F and Rossi G 1994 *Phys. Rev.* B **49** 15682
[10] Sirotti F, Panaccione G and Rossi G 1995 *Phys. Rev.* B **52** R17063
[11] Hillebrecht F U, Rose H B, Kinoshita T, Idzerda Y U, van der Laan G, Denecke R and Ley L 1995 *Phys. Rev. Lett.* **75** 2883
[12] Schellenberg R, Kisker E, Fanelsa A, Hillebrecht F U, Menchero J G, Kaduwela A P and Fadley C S 1998 *Phys. Rev.* B **57** 14310
[13] van der Laan G 1997 *Phys. Rev.* B **55** 3656
[14] Thole B T and van der Laan G 1991 *Phys. Rev.* B **44** 12424
[15] van der Laan G and Thole B T 1993 *Phys. Rev.* B **48** 210
[16] Thole B T and van der Laan G 1994 *Phys. Rev.* B **49** 9613
[17] van der Laan G 1995 *Phys. Rev.* B **51** 240
[18] Cowan R D 1981 *The Theory of Atomic Structure and Spectra* (Berkeley, CA: University of California Press)
[19] van der Laan G, Arenholz E, Navas E, Bauer A and Kaindl G 1996 *Phys. Rev.* B **53** R5998
[20] Torelli P 1998 *Thesis* Università di Modena